Article:
Green, A.C., Rudolph-Stringer, V., Straszkowski, L. et al. (2018) Retinoic acid receptor γ activity in mesenchymal stem cells regulates endochondral bone, angiogenesis, and B lymphopoiesis. Journal of Bone and Mineral Research, 33 (12). pp. 2202-2213. ISSN: 0884-0431

https://doi.org/10.1002/jbmr.3558

Disclosures

The authors have declared that no conflict of interest exists.

Abstract

Retinoic acid receptor (RAR) signaling regulates bone structure and hematopoiesis through intrinsic and extrinsic mechanisms. This study aimed to establish how early in the osteoblast lineage loss of *Rarg* disrupts the bone marrow microenvironment. Bone structure was analyzed by microCT in $Rarg^{-/-}$ mice and mice with *Rarg* conditional deletion in *Osterix-Cre*-targeted osteoblast progenitors or *Prrx1-Cre*-targeted mesenchymal stem cells. $Rarg^{-/-}$ tibiae exhibited less trabecular and cortical bone and impaired longitudinal and radial growth. The trabecular bone and longitudinal, but not radial, growth defects were recapitulated in $Prrx1{:}Rarg^{\Delta/\Delta}$ mice but not $Osx1{:}Rarg^{\Delta/\Delta}$ mice. While both male and female $Prrx1{:}Rarg^{\Delta/\Delta}$ mice had low trabecular bone mass, males exhibited increased numbers of trabecular osteoclasts and $Prrx1{:}Rarg^{\Delta/\Delta}$ females had impaired mineral deposition. Both male and female $Prrx1{:}Rarg^{\Delta/\Delta}$ growth plates were narrower than controls and their epiphyses contained hypertrophic chondrocyte islands. Flow cytometry revealed that male $Prrx1{:}Rarg^{\Delta/\Delta}$ bone marrow exhibited elevated pro-B and pre-B lymphocyte numbers, accompanied by increased *Cxcl12* expression in bone marrow cells. $Prrx1{:}Rarg^{\Delta/\Delta}$ bone marrow also had elevated megakaryocyte-derived *Vegfa* expression accompanied by smaller sinusoidal vessels. Thus, RARγ expression by *Prrx1-Cre*-targeted cells directly regulates endochondral bone formation and indirectly regulates tibial vascularization. Furthermore, RARγ expression by *Prrx1-Cre*-targeted cells extrinsically regulates osteoclastogenesis and B lymphopoiesis in male mice.

Keywords: Genetic animal models, osteoimmunology, osteoblasts, stromal/stem cells, tissue signaling – other (retinoic acid receptor signaling)

Introduction

The skeleton is a dynamic organ that is constantly remodeled to maintain its structural integrity. The medullary cavity of bones contains bone marrow (BM), which is the primary post-natal site of hematopoiesis. Microenvironments in the BM are comprised of multiple cell types that influence each other to regulate both hematopoiesis and bone formation and resorption. These cell types include mesenchymal stem cells, osteoblast-lineage cells, perivascular cells, endothelial cells, adipocytes and hematopoietic cells including osteoclasts and immune cells. Previous studies have found that deletion of retinoic acid receptor γ (RARγ) resulted in mice with low bone mass and hematopoietic defects that were, at least in part, induced by non-hematopoietic cells (1, 2). Thus, while RARγ has direct roles in hematopoiesis (intrinsic regulation), RARγ signaling in non-hematopoietic cells in the BM microenvironment also influences hematopoiesis (extrinsic regulation).

RARs are nuclear receptors that regulate transcription of genes and have important roles in the proliferation and differentiation of many cell lineages. There are three subtypes of RARs; α, β and γ, that can have either distinct or equivalent functions in different cell lineages (3). *Rara*$^{-/-}$ and *Rarg*$^{-/-}$ mice have defects in multiple tissues and were initially reported to exhibit neonatal lethality (4, 5). The housing of these mice in a clean animal facility improved survival, especially for *Rara*$^{-/-}$ mice. While *Rarg*$^{-/-}$ mice still showed significant post-natal lethality in cleaner housing conditions, some survived up to 12 months of age (6). Eight-week-old *Rara*$^{-/-}$ mice displayed no defects in bone (1) or hematopoiesis (6, 7). In comparison, histomorphometric analysis of tibiae from 8-week-old *Rarg*$^{-/-}$ mice revealed they had less trabecular bone when compared to wild type littermates, and in males this was associated with increased osteoclastogenesis (1).

In addition to lower bone mass, *Rarg*$^{-/-}$ mice developed a myeloproliferative-like syndrome (MPS) characterized by significantly more granulocytes in the peripheral blood (PB), BM and

spleen (2). *Rarg*$^{-/-}$ mice also exhibited defects in erythropoiesis and B lymphopoiesis (2, 8), with lower numbers of pro-B and pre-B lymphocytes in the BM (9). When BM from wild type mice was transplanted into mice with a *Rarg*$^{-/-}$ microenvironment, the transplanted mice rapidly developed the MPS-like disease and the erythrocyte and B lymphocyte defects. In comparison, when *Rarg*$^{-/-}$ BM was transplanted into wild type mice these hematopoietic defects were resolved. This indicated that RARγ expression in microenvironment cells (extrinsic) was essential for normal hematopoiesis, and that the mature hematopoietic cell defects observed in *Rarg*$^{-/-}$ mice were not due to intrinsic loss of RARγ in those cells.

We have recently shown that deletion of *Rarg* in primitive *nestin-Cre*-targeted neural crest-derived mesenchymal stem cells (MSCs) and their progeny impaired BM B lymphopoiesis and thymic T lymphopoiesis (9). The defects observed in *nestin-Cre:Rarg*$^{\Delta/\Delta}$ mice did not fully recapitulate all hematopoietic phenotypes exhibited by *Rarg*$^{-/-}$ mice, suggesting that additional cells within the microenvironment regulate hematopoiesis via the actions of RARγ. Since osteoblast-lineage cells play a key role in supporting B lymphopoiesis (10-12), and *Rarg* is expressed throughout osteoblast differentiation (13)**,** we sought to investigate the role of RARγ at different stages of osteoblast commitment in the regulation of bone structure and hematopoiesis.

To determine whether committed osteoblast-lineage cells were involved in inducing changes to bone mass and hematopoiesis we conditionally deleted *Rarg* in osteoblast progenitors (OPs) and their progeny using *Osx1-Cre* and compared their phenotype to mice with targeted deletion in more primitive limb bud-derived MSCs and their progeny using *Prrx1-Cre* (also known as *Prx1*). Here we report a role for *Rarg* signaling in *Prrx1-Cre*-targeted limb bud-derived mesenchymal cells, but not in *Osx1-Cre*-targeted osteoprogenitor cells, in the regulation of endochondral bone, sinusoidal vessels and B lymphopoiesis.

Methods

Mice

All experiments were approved by the St. Vincent's Health Melbourne Animal Ethics Committee and conducted in strict compliance to the regulatory standards of the Australian Code of Practice for the Care and Use of Animals for Scientific Purposes. Tibiae were obtained from 8- and 12-week-old male and female *Rarg*$^{-/-}$ [Rarg^{tm1Ipc}] and *Rarg*$^{+/+}$ littermate mice (4). *Rarg* was conditionally deleted in OPs using *Osx1-GFP::Cre* [B6.Cg-Tg(Sp7-tTA,tetO-EGFP/cre)1Amc/J] (14) and in limb bud-derived mesenchymal stem cells using *Prrx1-Cre* mice [B6.Cg-Tg(Prrx1-cre)1Cjt/J] (15), each of these crossed with *Rarg*$^{fl/fl}$ mice [Rarg^{tm3Ipc}] (16). In all studies 12-week-old *Cre*$^{+}$*:Rarg*$^{+/+}$ mice were used as controls for 12-week-old *Cre*$^{+}$*:Rarg*$^{fl/fl}$ mice. *Osx1-GFP::Cre*$^{+}$*Rarg*$^{fl/fl}$ mice are referred to as *Osx1:Rarg*$^{\Delta/\Delta}$, *Osx1-GFP::Cre*$^{+}$*Rarg*$^{+/+}$ as *Osx1:Rarg*$^{+/+}$, *Prrx1-Cre*$^{+}$*:Rarg*$^{fl/fl}$ as *Prrx1:Rarg*$^{\Delta/\Delta}$ and *Prrx1-Cre*$^{+}$*:Rarg*$^{+/+}$ as *Prrx1:Rarg*$^{+/+}$. All mice were fully backcrossed onto the C57BL/6 strain prior to use in these studies. *Prrx1:Rarg* mice were crossed with *Rosa26-loxP-stop-loxP*-enhanced yellow fluorescent protein (*R26-stop*-EYFP; B6.129X1-*Gt(ROSA)26Sor*$^{tm1(EYFP)Cos}$/J) mice for these studies. *Prrx1-Cre* mice occasionally exhibit germline activation of Cre (15). To exclude these mice from analysis germline activation was identified by EYFP expression in peripheral blood (PB) cells by flow cytometry for all *Prrx1-Cre*$^{+}$ mice. In *Prrx1:Rarg*$^{\Delta/\Delta}$ mice, excision of *Rarg* exon 8 was also confirmed to be specific to non-hematopoietic tissues by genomic PCR of PB (forward primer: tcttacctgctgagtcccaaccaa, reverse primer: agaagaaagcagttacagggcagg).

Micro-computed tomography

Bone structure of tibiae from 8-week-old *Rarg* mice [to compare to previous work (1)] and adult 12-week-old *Rarg*, *Osx1:Rarg* and *Prrx1:Rarg* mice were analysed by μCT. Tibiae were

dissected, cleaned of muscle and connective tissue, fixed in 2% paraformaldehyde overnight at 4°C then stored in 70% ethanol. The SkySkan 1076 system (Bruker-microCT, Kontich, Belgium) was used to scan tibiae, following standard guidelines (17). The image acquisition parameters used were: 9 μm voxel resolution, 0.5 mm aluminum filter, 45 kV voltage and 100 μA current, 2300 ms exposure time, 0.5° rotation step and frame averaging of 1. Reconstruction and analysis of images was performed using SkyScan software NRecon (1.6.9.8), DataViewer (1.5.0) and CTAnalyser (1.13.11.0). The region of interest (ROI) for tibial trabecular bone was identified as a 3% distal offset from the growth plate and a height of 13.5% of total tibial length. Trabecular bone was analyzed utilizing adaptive thresholding for all samples; minimum values were 45 (*Rarg*), 44 (*Osx1:Rarg*), 51 (*Prrx1:Rarg*) and maximum of 225. Region of interests for cortical bone were defined as a 40% distal offset from the growth plate and 13.5% region of total tibial length. Global automatic thresholding was used for cortical bone analysis with a minimum of 95 (*Rarg, Osx1:Rarg*) or 100 (*Prrx1:Rarg*) and a maximum of 225.

Histomorphometry, immunohistochemistry and immunofluorescence

Tibiae were embedded in methylmethacrylate and 5 μm sections were stained with toluidine blue as previously described (1, 18). Histomorphometry of the secondary spongiosa was performed using OsteoMeasure7 v4.1.1.2 (OsteoMetrics, Atlanta, GA, USA) using standard guidelines (19). The region analyzed was 370 μm distal to the base of the growth plate using a 370 μm^2 box from the edge of the marrow cavity excluding all cortical bone in 3 non-overlapping rows.

Cartilage and sinusoidal vessels were analyzed on decalcified tibial sections as previously described (20). Tibiae were fixed in 2% paraformaldehyde overnight, decalcified by replacing the EDTA solution twice over 2 weeks. Samples were processed and embedded in paraffin,

5µm sections were dewaxed and rehydrated. To analyze sinusoidal vessels, samples were stained for VEGFR-3 (eBioscience) at [1:400] as previously described (20). To analyze the growth plate, samples were stained with Safranin-O and Fast Green as previously described (21). The numbers and sizes of VEGFR-3+ sinusoidal vessels and sinusoid perimeter in the secondary spongiosa, in addition to growth plate height and the number of epiphyseal hypertrophic chondrocyte islands were measured using OsteoMeasure software (20). The growth plate proliferative versus hypertrophic zones could not be distinguished, so separate samples were collected at 20 days of age to allow assessment of these zones according to standard protocols using OsteoMeasure software (22).

Mouse tibiae were prepared following the protocol described by Poulton *et al.* (23, 24). Immunofluorescence labelling protocol for formalin-fixed, paraffin-embedded tissue was adapted from Nolan *et al.* (25). Antibodies, detection and labelling conditions are found in Supplemental Table 2. Endogenous peroxidase activity was blocked with 3% H_2O_2 (Merck, MA, USA) for 30 mins, washed in Tris-buffered saline (TBS), followed by a protein block with TNB blocking solution (Perkin Elmer, MA, USA) for 1 hour prior to primary antibody incubation (Supplemental Table 2). All washes were performed three times with TBS for 5 mins each. Multiplexed immunofluorescence labelling was done through sequential staining as described previously (24). After antibody staining, sections were counterstained with DAPI (1:1000) for 5 mins and mounted in Citifluor hard set mounting media CFPVOH plus AF100 (Citifluor, PA, USA). Whole slide scans were imaged on the Vectra Polaris Quantitative Pathology Imaging System (Perkin Elmer).

Hematological analysis

PB was obtained by retro-orbital bleeding, BM was flushed from one femur, spleens were

crushed and filtered to single cell suspensions. Hematopoietic cellularity was assessed with a Sysmex KX-21N analyzer (Sysmex, Kobe, Japan). BM cells were stained with fluorophore-conjugated antibodies (Supplementary Table 1) (26), all flow cytometry data were collected using a Becton Dickinson (BD) LSR Fortessa (BD Bioscience) and data analyzed using FlowJo 8.8.7 (Treestar, Ashland, OR, USA).

Analysis of primary osteoblast-lineage cells

Osteoblast-lineage cells were isolated from *Prrx1:Rarg* long bones as previously described (13). Briefly, bones were cleaned, cut into 1 mm^2 pieces and gently crushed using a mortar and pestle. Bone marrow was removed by washing fragments with 2% FBS and 5 mM EDTA in PBS. Bone fragments (containing trabecular and cortical bone) were digested with 3 mg/ml collagenase type 1 (Worthington) in PBS for 45 minutes at 37°C with agitation and stained with fluorophore-conjugated antibodies (Supplementary Table 1). Non-viable, hematopoietic (CD45, Ter119) and endothelial (CD31) cells were omitted, MSCs (Sca-1^+, $CD51^+$) and osteoblast-lineage cells (Sca-1^-, $CD51^+$) were sorted on a BD Influx (BD Bioscience) (13).

RNA isolation and qPCR

Total RNA was isolated using an Isolate II RNA Micro Kit (Bioline) and cDNA synthesized using AffinityScript qPCR cDNA Synthesis Kit (Agilent Technologies, Santa Clare, CA, USA) as per manufacturers' instructions. qPCR was performed using Brilliant II SYBR green (Agilent Technologies) and 5 pmol of primers [all reported previously (1, 26, 27)] using a MxPro 3000P Stratagene system and software.

Statistics

Data are presented as mean ± SD and statistical analysis was performed using an unpaired two-tailed Student's t-test in Prism 7 (Graphpad Software, La Jolla, CA, USA).

Results

Rarg$^{-/-}$ mice have less trabecular bone

MicroCT analysis of 8- and 12-week-old *Rarg* mice confirmed the findings of our previous study that used histomorphometric analysis (1). In 8- and 12-week-old *Rarg$^{-/-}$* tibiae, trabecular bone volume was 72% and 62% lower in males and 42% and 58% lower in females compared to *Rarg$^{+/+}$* mice (Fig. 1 and Supplemental Fig. 1 show 12- and 8-week-old data, respectively). There were no changes in trabecular thickness in *Rarg$^{-/-}$* mice (Fig. 1B, Supplemental Fig 1B). However, trabecular separation was significantly higher (Fig. 1C, Supplemental Fig. 1C) and trabecular number was significantly lower in both male and female *Rarg$^{-/-}$* mice compared to their sex-matched controls (Fig. 1D, Supplemental Fig. 1D). The lower trabecular bone mass in *Rarg$^{-/-}$* mice is shown in reconstructed images of 3D trabecular bone stucture (Fig. 1E-H, Supplemental Fig. 1E-H).

Rarg$^{-/-}$ mice have impaired bone growth

Tibiae of 8- and 12-week-old *Rarg$^{-/-}$* mice were >12% shorter compared to *Rarg$^{+/+}$* mice (Supplemental Fig. 1I, Fig. 1I), indicating impaired longitudinal growth of tibiae. μCT analysis found no change in cortical bone parameters in 8-week-old female mice, consistent with our previous histomorphometric analysis (1) (Supplemental Fig. **1**J-M). However, 8-week-old male and all 12-week-old *Rarg$^{-/-}$* mice had thinner cortical bone compared to *Rarg$^{+/+}$* mice (Supplemental Fig. 1J, Fig. 2A). These mice also had a significantly smaller cortical area and periosteal perimeter (Supplemental Fig. 1L-M, Fig. 2C-D), indicating impaired radial growth. 12-week old *Rarg$^{-/-}$* females also had a greater marrow area (Fig. 2B).

Osx1:Rarg$^{\Delta/\Delta}$ mice have no change in bone volume

We next sought to identify which osteoblast precursor population is important for maintaining trabecular and cortical bone mass via RARγ signaling. *Rarg$^{-/-}$* male mice exhibited increased osteoclastogenesis *in vivo,* yet RAR inhibition blocked osteoclast differentiation of mouse whole BM cells and RAW264.7 cells *in vitro* (1). Osteoclast formation is commonly regulated by osteoblast-lineage cells via their production of RANKL and OPG (28), therefore we investigated the bone phenotype in mice with *Rarg* deletion in the osteoblast lineage, directed with *Osx1-Cre*. Analysis of 12-week-old male tibiae by μCT found no changes in trabecular bone structure in the secondary spongiosa (Fig. 3A-F). Analysis of cortical bone similarly identified no significant differences between *Osx1:Rarg$^{\Delta/\Delta}$* and *Osx1:Rarg$^{+/+}$* mice and tibial length was unchanged by *Rarg* targeting (Supplemental Fig. 2A-G). Hence loss of *Rarg* from *Osx1-Cre*-targeted OPs and their progeny is not the cause of the bone defects observed in *Rarg$^{-/-}$* mice.

Prrx1:Rarg$^{\Delta/\Delta}$ mice have reduced trabecular bone

We deleted *Rarg* in primitive limb bud-derived mesenchymal stem cells and their progeny using *Prrx1-Cre* to determine if an earlier mesenchymal cell might mediate the impaired bone growth and lower trabecular bone mass observed with global loss of *Rarg*. *Prrx1:Rarg$^{\Delta/\Delta}$* male and female mice had significantly less trabecular bone compared to age- and sex-matched *Prrx1:Rarg$^{+/+}$* mice (Fig. 4A, E-H). Trabecular thickness was unchanged (Fig. 4B) but *Prrx1:Rarg$^{\Delta/\Delta}$* males had significantly greater trabecular separation (Fig. 4C) and both male and female *Prrx1:Rarg$^{\Delta/\Delta}$* mice had lower trabecular number than controls (Fig. 4D). These changes to trabecular bone mimicked those observed in *Rarg$^{-/-}$* mice, although the difference in bone mass was more variable in males. The low trabecular bone mass was more pronounced

in *Prrx1:Rarg*$^{\Delta/\Delta}$ males than females, consistent with observations in *Rarg*$^{-/-}$ mice [(1) and Fig. 1]. The tibiae were shorter in *Prrx1:Rarg*$^{\Delta/\Delta}$ compared to *Prrx1:Rarg*$^{+/+}$ mice (Fig. 4I), however, no differences in cortical bone structure were observed between *Prrx1:Rarg*$^{\Delta/\Delta}$ and *Prrx1:Rarg*$^{+/+}$ mice (Supplemental Fig. 3), indicating that longitudinal, but not radial, growth was impaired.

Prrx1:Rarg$^{\Delta/\Delta}$ *females exhibit more trabecular osteoblasts and males have more trabecular osteoclasts*

In female *Prrx1:Rarg*$^{\Delta/\Delta}$ mice, histomorphometric analysis revealed that the low bone volume was accompanied by a greater proportion of unmineralized bone (osteoid) in the trabecular bone (Fig. 5A). Female *Prrx1:Rarg*$^{\Delta/\Delta}$ mice had a significantly higher percentage of bone comprising osteoid due to a greater proportion of osteoid-covered bone surface (Fig. 5A-B) rather than a significant change in osteoid thickness (Fig. 5C). Female *Prrx1:Rarg*$^{\Delta/\Delta}$ mice also had more osteoblasts than controls (Fig. 5E), and although most *Prrx1:Rarg*$^{\Delta/\Delta}$ females had a higher osteoblast surface this was not statistically significant (Fig. 5D).

In contrast to female mice, male *Prrx1:Rarg*$^{\Delta/\Delta}$ mice displayed no significant changes in trabecular osteoid surface, osteoblast numbers or osteoblast surface compared to age-matched *Prrx1:Rarg*$^{+/+}$ mice (Fig. 5A-E). Instead, male *Prrx1:Rarg*$^{\Delta/\Delta}$ mice exhibited greater osteoclast surface and osteoclast numbers in trabecular bone compared to *Prrx1:Rarg*$^{+/+}$ males (Fig. 5F-G). These data have revealed that *Rarg* deletion in very primitive cells of the osteoblast lineage is the major contributor to the bone phenotype in *Rarg*$^{-/-}$ mice and that the cellular mechanisms by which RARγ regulates trabecular bone mass are either different in males and females or predominate to different extents in males and females.

Further investigation of tibial sections revealed islands of hypertrophic chondrocytes in the epiphyseal trabecular bone of both male and female *Prrx1:Rarg*$^{\Delta/\Delta}$ mice (Fig. 5H-K). When quantified, chondrocyte islands were present in the majority of *Prrx1:Rarg*$^{\Delta/\Delta}$ mice but only in one *Prrx1:Rarg*$^{+/+}$ male mouse. This suggests their impaired growth relates to a delay in establishment of the secondary ossification center. Furthermore, the growth plates of *Prrx1:Rarg*$^{\Delta/\Delta}$ male and female mice were 14.8% and 16.3% shorter than controls (Fig. 5L), respectively, correlating with the impaired bone growth in these mice and the high level of RARγ expression in the murine growth plate (29). Surprisingly, when the growth plates of young (20 day old) *Prrx1:Rarg*$^{\Delta/\Delta}$ male and female mice were assessed, this difference in growth plate width was not present, but the proliferative zone (Fig. 5M) was of normal width and the hypertrophic zone width was extended (Fig. 5N). The hypertrophic chondrocytes also appeared larger in size (Fig. 5O, P). This suggested that both the reduction in bone length, and the presence of cartilage islands within the secondary ossification center may relate to an extension in the period of hypertrophy. This was clearly transient, and was followed by an early reduction in growth plate width.

Prrx1:Rarg$^{\Delta/\Delta}$ *male mice demonstrated altered bone marrow B lymphopoiesis*

We sought to determine whether *Prrx1:Rarg*$^{\Delta/\Delta}$ mice also had microenvironment-induced alterations in hematopoietic cells. Hematological analysis revealed that *Prrx1:Rarg*$^{\Delta/\Delta}$ males, but not females, exhibited a significant increase in BM leukocytes (Fig. 6A). To further investigate the altered leukocyte numbers in *Prrx1:Rarg*$^{\Delta/\Delta}$ males, BM samples were profiled by flow cytometry (Fig. 6B-C). In *Prrx1:Rarg*$^{\Delta/\Delta}$ males there was a significant increase in the numbers of BM-derived $B220^{+}IgM^{-}$ cells, with no changes in the numbers of $B220^{+}IgM^{+}$ B lymphocytes (identifying a mix of BM-derived immature B lymphocytes and recirculating mature B lymphocytes) (Fig. 6D). Further investigation revealed that within the $B220^{+}IgM^{-}$

population (Fig. 6C) there was an increase in the numbers of both $CD19^+CD43^+$ pro-B lymphocytes and $CD19^+CD43^-$ pre-B lymphocytes, but no change in the numbers of $CD19^-CD43^+$ pre-pro-B lymphocytes in *Prrx1:Rarg*$^{\Delta/\Delta}$ compared to *Prrx1:Rarg*$^{+/+}$ male mice (Fig. 6E). Thus the enhanced formation of early B lymphocyte precursors originated at the pro-B lymphocyte stage but did not affect maturing ($B220^+IgM^+$) B lymphocyte numbers (Fig. 6F). The hematopoietic phenotype was sex-specific as there were no changes in BM B lymphocytes in female *Prrx1:Rarg*$^{\Delta/\Delta}$ mice (Supplemental Fig. 4). We also confirmed that *Prrx1-Cre* did not target the B lymphocytes, with no co-expression of B220 and EYFP observed in immunofluorescence studies of tibiae or flow cytometry analysis of the peripheral blood of the mice (Supplemental Fig. 5). Furthermore, there were no differences in the numbers of PB (Supplemental Fig. 4) or splenic (data not shown) B lymphocytes in male or female *Prrx1:Rarg*$^{\Delta/\Delta}$ mice. Aside from an increase in BM granulocytes in female *Prrx1:Rarg*$^{\Delta/\Delta}$ mice, no other significant differences were detected in the other hematopoietic cell populations (data not shown).

Our data suggested that *Prrx1-Cre* targets cells that are involved in the regulation of B lymphopoiesis, thus we investigated the gene expression of key factors involved in this process (30, 31) in whole BM cells. The expression of *Cxcl12,* tumor necrosis factor receptor superfamily member 11b (*Tnfrsf11b*; OPG) and *Vegfa* were significantly higher in *Prrx1:Rarg*$^{\Delta/\Delta}$ mice, *Flt3l* was unchanged (Fig. 6G-J) and *Tnfsf11* (RANKL), *Kitl* and *Il7* could not be detected. To determine if mesenchymal cells were the sources of the altered transcripts, osteoblastic cells were purified by FACS into *Prrx1:*$EYFP^+$ MSCs (lineage, CD45 and CD31 negative, Sca-1^+, $CD51^+$) and osteoblast-lineage cells (lineage, CD45 and CD31 negative, Sca-1^-, $CD51^+$) from *Prrx1:Rarg*$^{+/+}$ and *Prrx1:Rarg*$^{\Delta/\Delta}$ mice. qPCR revealed different changes in gene expression in purified *Prrx1:Rarg*$^{\Delta/\Delta}$ osteoblastic populations compared to whole BM cells. The expression of *Cxcl12*, the secreted and membrane forms of Kit ligand (*Kitl*) and *Flt3l*

were significantly lower in *Prrx1:Rarg*$^{\Delta/\Delta}$ MSCs compared to *Prrx1:Rarg*$^{+/+}$ MSCs (Fig. 6K). All other transcripts were unaltered in MSCs (Fig. 6K), with the exception of *Il7* and *Tnfsf11*, which were not detected. Furthermore, *Cxcl12*, secreted *Kitl* and *Il7* were significantly reduced in *Prrx1:Rarg*$^{\Delta/\Delta}$ osteoblast-lineage cells whereas all other transcripts were unaltered (Fig. 6L), with the exception of *Tnfsf11* which could not be detected (data not shown).

Prrx1:Rarg$^{\Delta/\Delta}$ *mice altered bone marrow vascularization*

Endochondral bone formation is tightly linked to BM angiogenesis and sinusoidal vessels are important constituents of the BM microenvironment. Given that *Vegfa* expression was increased in the BM of *Prrx1:Rarg*$^{\Delta/\Delta}$ mice and is a key regulator of BM angiogenesis, we quantified the numbers of sinusoidal vessels in the BM of the secondary spongiosa by histomorphometry. The number of sinusoids in the BM was increased in *Prrx1:Rarg*$^{\Delta/\Delta}$ females (Fig. 7A, G-H). In both male and female *Prrx1:Rarg*$^{\Delta/\Delta}$ mice the sinusoids were smaller (Fig. 7B, E-H). The sinusoids occupied less space within the BM in male *Prrx1:Rarg*$^{\Delta/\Delta}$ mice (Fig. 7B-C), reflecting the sinusoidal vessel constriction. In contrast, the sinusoid perimeter per marrow area was unchanged (Fig. 7D). The vessel phenotype was reflected throughout the BM including in the primary spongiosa (data not shown).

To determine the source of the increased *Vegfa* observed in the BM we performed immunofluorescence studies, investigating the co-expression of the *Prrx1-Cre*-targeted cells (using an antibody against EYFP), and Vegf-a in tibiae sections from *Prrx1:Rarg*$^{\Delta/\Delta}$ and *Prrx1:Rarg*$^{+/+}$ mice. Vegf-a was highly expressed in the growth plate of *Prrx1:Rarg*$^{+/+}$ mice (Fig. 7I), consistent with a previous report showing Vegf-a expression in this region (32). In contrast, the production of Vegf-a was significantly reduced in the growth plate of *Prrx1:Rarg*$^{\Delta/\Delta}$ mice, but increased in the bone marrow megakaryocytes (Fig. 7J). Flow cytometry-based quantitation studies showed that the proportions of CD41+ megakaryocytes

were unaltered in the bone marrow of *Prrx1:Rarg*$^{\Delta/\Delta}$ compared to *Prrx1:Rarg*$^{+/+}$ mice (Fig. 7K).

Discussion

This study has identified that RARγ activity in *Prrx1-Cre*-targeted cells is a key regulator in the formation of a healthy BM microenvironment, significantly influencing the development of normal trabecular bone mass, angiogenesis and B lymphopoiesis.

Loss of *Rarg* in *Prrx1-Cre*-targeted cells and their progeny resulted in similar (albeit less severe) changes to trabecular bone and longitudinal bone growth as $Rarg^{-/-}$ mice. The bone phenotypes were not observed when *Rarg* was deleted in *Osx1-Cre*-targeted early osteoblast progenitor cells (and also a subset of hypertrophic chondrocytes), confirming that this role of *Rarg* is mediated by a non-overlapping population of immature mesenchymal cells targeted by *Prrx1-Cre*. Deletion of *Rarg* in *Prrx1-Cre*-targeted cells also influenced growth plate chondrocyte hypertrophy preceding the trabecular bone defects and abnormal BM vascularization in $Prrx1{:}Rarg^{\Delta/\Delta}$ mice.

$Prrx1{:}Rarg^{\Delta/\Delta}$, but not $Osx1{:}Rarg^{\Delta/\Delta}$, mice had defects in trabecular bone mass, similar to that observed in $Rarg^{-/-}$ mice. *Prrx1-Cre* and *Osx1-Cre* both target cells that give rise to the osteoblast lineage, however their expression patterns vary between anatomical sites and the other mesenchymal lineages they form. In *Prrx1-Cre* mice, Cre recombinase (Cre) is expressed in the multipotent cells of the limb bud mesenchyme, flank mesoderm and craniofacial mesenchyme, i.e. in the appendicular skeleton, some calvarial bones and the sternum but not in the vertebrae (15). This means that genes deleted from $Prrx1\text{-}Cre^{+}$ multipotent cells will remain deleted in their progeny. In the BM of long bones, 50% of $Prrx1\text{-}Cre^{+}$ cells are $PDGFR\alpha^{+}Sca\text{-}1^{+}$ (PαS) cells (a population enriched with MSCs) and $Prrx1\text{-}Cre^{+}$ cells give rise to osteoblasts/osteocytes, CXCL12-abundant reticular (CAR) cells, adipocytes and chondrocytes, but not hematopoietic or endothelial cells (33, 34). Thus, the changes observed in $Prrx1{:}Rarg^{\Delta/\Delta}$ bones could be due to loss of *Rarg* in any of these cell types or combinations

of cells. In comparison, *Osx1-Cre* only targets a small proportion of PαS cells (~5%) (33) and is expressed in more differentiated early OPs that give rise to osteoblasts residing in the perichondrium, periosteum, endosteum and trabecular bone as well as osteocytes (14, 35, 36). In addition to the osteoblast lineage, *Osx1-Cre* is expressed in some growth plate prehypertrophic and hypertrophic chondrocytes, perivascular cells (including CAR cells) and BM adipocytes post-natally (33, 35, 37). The lack of a bone phenotype in *Osx1:Rarg*$^{\Delta/\Delta}$ mice suggests that the bone defects following deletion of *Rarg* are not due to lack of *Rarg* in cells committed to the osteoblast lineage. Thus, the regulation of bone length and trabecular bone mass via RARγ activity appears to occur in MSCs (or potentially their immature progeny).

Deletion of RARs using *Col2a1-Cre*, which targets chondrocytes, osteoblasts and synovial fibroblasts (38, 39), has also been shown to alter endochondral bone growth (29). *Col2a1-Cre*$^{+}$*:Rara*$^{fl/fl}$*Rarg*$^{fl/fl}$ mice and *Col2a1-Cre*$^{+}$*:Rarb*$^{fl/fl}$*Rarg*$^{fl/fl}$ mice were reported to have low trabecular bone mass, but this was not quantitated (29), so we cannot reliably compare that aspect of the phenotype to our models. However, *Col2a1-Cre*$^{+}$*:Rara*$^{fl/fl}$*Rarg*$^{fl/fl}$ mice and *Col2a1-Cre*$^{+}$*:Rarb*$^{fl/fl}$*Rarg*$^{fl/fl}$ mice, but not *Col2a1-Cre*$^{+}$*:Rara*$^{fl/fl}$*Rarb*$^{fl/fl}$ mice had narrow growth plates and exhibited impaired long bone growth (29). In the growth plates of these mice the hypertrophic zone appeared largely unaffected, but chondrocyte proliferation was impaired. This aberrant functioning of the growth plate impaired endochondral bone formation, resulting in a lower trabecular bone mass in *Col2a1-Cre*$^{+}$*:Rara*$^{fl/fl}$*Rarg*$^{fl/fl}$ mice and *Col2a1-Cre*$^{+}$*:Rarb*$^{fl/fl}$*Rarg*$^{fl/fl}$ mice. The bone phenotype of *Col2a1-Cre*$^{+}$*:Rarg*$^{fl/fl}$ mice was not assessed, however, given that mice lacking *Rara* and *Rarb* in *Col2a1-Cre*-targeted chondrocytes appeared phenotypically normal, loss of RARγ is likely to be the main contributor to the phenotypes observed in the *Col2a1-Cre*$^{+}$*:Rara*$^{fl/fl}$*Rarg*$^{fl/fl}$ and *Col2a1-Cre*$^{+}$*:Rarb*$^{fl/fl}$*Rarg*$^{fl/fl}$ mice.

If *Rarg* expression in differentiating chondrocytes is required for normal growth plate function and subsequent endochondral bone formation and long bone growth, this could contribute to both the trabecular bone and longitudinal growth defects observed in *Prrx1:Rarg*$^{\Delta/\Delta}$ mice, because chondrocytes are targeted by *Prrx1*. Indeed, in *Prrx1:Rarg*$^{\Delta/\Delta}$ mice the growth plate showed early abnormalities in hypertrophy, and in adult bones was shorter than that of controls, suggesting a potential cause of the impaired longitudinal growth. Intriguingly, *Prrx1:Rarg*$^{\Delta/\Delta}$ mice also exhibited islands of hypertrophic chondrocytes trapped in the trabecular bone in the epiphysis of tibiae; this also suggests an extension of the hypertrophic stage. Cartilage remnants have similarly been observed in diaphyseal trabecular bone of *Osx1-Cre:EphrinB2*$^{\Delta/\Delta}$ mice and occur due to defective osteoclastic resorption in the primary ossification center (40). Similarly, children with osteogenesis imperfecta also contain cartilage within their bones after treatment with anti-resorptive bisphosphonate therapy (41). The presence of an extended hypertrophic zone at the growth plate, and hypertrophic chondrocyte islands in *Prrx1:Rarg*$^{\Delta/\Delta}$ mice thus suggests that chondrocyte hypertrophy may progress more slowly leading to impaired resorption of the secondary ossification center.

One factor that plays a role in endochondral ossification and therefore long bone growth and trabecular bone formation is Vegf-a, which may contribute to the phenotype in *Prrx1:Rarg*$^{\Delta/\Delta}$ mice. Vegf-a plays an essential role in the neovascularization of cartilage, facilitating endochondral bone formation (42, 43). In the BM, Vegf-a is expressed by osteoblast-lineage cells, hypertrophic chondrocytes and some proliferating chondrocytes (42, 44)**,** and some hematopoietic cells, including myeloid progenitors and megakaryocytes (45). Vegf-a stimulates the recruitment of endothelial cells for vessel formation, which in turn recruits osteoclasts and osteoblasts to the growth plate to resorb and replace cartilage with mineralized bone (46). As expected, the increased *Vegfa* expression in the BM *Prrx1:Rarg*$^{\Delta/\Delta}$ female mice was accompanied by significantly more sinusoidal vessels in the BM secondary spongiosa,

however, the sinusoids were constricted, resulting in significantly reduced overall vessel area in the BM compared to *Prrx1:Rarg*$^{+/+}$ mice. This gain of function effect is the opposite of, and hence consistent with, reports of mice lacking 2 of the 3 VEGF isoforms; $VEGF_{164}$ and $VEGF_{188}$, but still expressing $VEGF_{120}$. These mice have fewer, more dilated blood vessels, indicating that the $VEGF_{164}$ and $VEGF_{188}$ isoforms are essential for BM vascularization (47). The sinusoidal vessels were similarly constricted in male *Prrx1:Rarg*$^{\Delta/\Delta}$ mice, however the vessel number was not increased. The normal number of sinusoidal vessels in the males may indicate that the excess Vegf-a is acting elsewhere in the BM. Furthermore, given *Vegfa* expression was unchanged in *Prrx1:Rarg*$^{\Delta/\Delta}$ MSCs and osteoblast-lineage cells isolated from collagenase-digested bone, the increased *Vegfa* in the BM must be derived from an alternate cell type**.** Indeed, our studies revealed that Vegf-a was upregulated in the megakaryocytes in the bone marrow of the *Prrx1:Rarg*$^{\Delta/\Delta}$ mice. Megakaryocytes and megakaryocyte cell lines have previously been shown to produce and secrete VEGF (48, 49). It is currently unclear as to why Vegf-a was increased in the megakaryocytes of *Prrx1:Rarg*$^{\Delta/\Delta}$ mice. However, the increased Vegf-a observed throughout the bone marrow correlated with the vascular changes we observed throughout the BM, whereas localized disruption to Vegf-a expression in chondrocytes of mice lacking leukemia inhibitory factor (LIF) results in enhanced vascularization localized to the growth plate (32).

Vegf-a also has direct effects on osteoclast precursors, increasing their expression of RANK (50) and enhancing osteoclastic differentiation, survival and resorptive activity (51). Furthermore, Gerber *et al.* found that inhibition of Vegf-a signaling in 24-day-old mice impaired vascularization and cartilage resorption (44). Thus in *Prrx1:Rarg*$^{\Delta/\Delta}$ males, it is likely that the increase in *Vegfa* contributed to the elevated trabecular osteoclasts and lower trabecular bone mass through the stimulation of osteoclast differentiation and recruitment, stimulation of cartilage and bone resorption, and/or prolonging the survival of trabecular osteoclasts. This

was consistent with the reduction in trabecular number accompanied by increased trabecular spacing but unaltered trabecular thickness in the *Prrx1:Rarg*$^{\Delta/\Delta}$ male mice, which is indicative of enhanced resorption. While the osteoclast numbers were unchanged in *Prrx1:Rarg*$^{\Delta/\Delta}$ females, the enhanced vascularization may have increased the osteoblast recruitment to the bone surface, contributing to the increased numbers of osteoblasts observed in these female mice.

Prrx1:Rarg$^{\Delta/\Delta}$ male mice also displayed altered B lymphopoiesis, indicating that RARγ signaling in *Prrx1-Cre*-targeted cells and/or their progeny are important BM microenvironment regulators of B lymphopoiesis. Male *Prrx1:Rarg*$^{\Delta/\Delta}$ mice had increased numbers of B lymphocyte precursors in the BM, with elevated pro-B and pre-B lymphocytes, but no changes in the more primitive pre-pro-B lymphocytes. Interestingly, the increase in immature B lymphocyte numbers were not reflected in mature B lymphocyte populations, because the numbers of immature B220^{+}IgM^{+} B lymphocytes, splenic and mature PB B lymphocytes were unchanged.

The upregulated *Cxcl12* expression in *Prrx1:Rarg*$^{\Delta/\Delta}$ male BM was consistent with the B lymphocyte phenotype observed in these mice. Cxcl12 is a positive regulator of B lymphopoiesis from the pre-pro-B to pre-B cell stages, hence could be contributing to the increased numbers of pro-B and pre-B lymphocytes observed in *Prrx1:Rarg*$^{\Delta/\Delta}$ male mice. The BM is the site of early B lymphopoiesis and distinct niches regulate different stages of development, including osteoblasts, osteoclasts, CAR cells, IL-7-expressing cells and endothelial cells. MSCs and osteoblast lineage cells play important roles in regulating early B lymphopoiesis (31). To determine if the increased expression of *Cxcl12*, or other potential B lymphocyte regulators, originated in *Prrx1*-derived mesenchymal cells, we FACS-isolated populations of MSCs (Sca-1^{+}, CD51^{+}) and osteoblast-lineage cells (Sca-1^{-}, CD51^{+}) from bone and examined their expression of known key B lymphocyte regulators. Surprisingly, many

regulatory genes were reduced in both MSCs (e.g. *Cxcl12*, *Kitl* and *Flt3*) and osteoblast-lineage cells (e.g. *Cxcl12*, *Kitl* and *Il7*), despite pro-B and pre-B cells being higher in *Prrx1:Rarg*$^{\Delta/\Delta}$ mice. This is the opposite to what we would expect if these cell types were regulating B lymphopoiesis in *Prrx1:Rarg*$^{\Delta/\Delta}$ mice as they are all identified as positive regulators of early B lymphopoiesis (31, 33, 52-55). This implies that other cell type(s) in the BM microenvironment are responsible for the increased B lymphocyte phenotype in these mice. These cells are likely to be the source of the increased *Cxcl12* expression in the BM in *Prrx1:Rarg*$^{\Delta/\Delta}$ male mice. Some candidates are chondrocytes (56) and endothelial cells (33), which have both been shown to express *Cxcl12*.

Another possible contributor to the increased pro-B and pre-B cells in the male *Prrx1:Rarg*$^{\Delta/\Delta}$ mice was the increased osteoclasts observed in these mice (31). Blin-Wakkach *et al.* showed that osteopetrotic *oc/oc* mice had impaired production of BM B lymphocytes from the pro-B cell stage (57) that was rescued by transplanting normal BM containing osteoclast precursors (58). Furthermore, administration of the anti-resorptive zoledronic acid (ZA) led to impaired B lymphopoiesis from the pre-pro-B lymphocyte stage, with no direct effect of ZA observed on the B lymphocyte cells (58). ZA treatment also dramatically reduced *Cxcl12* and *Il7* expression in CD45^{-} BM cells, which are devoid of most hematopoietic cells (58). Thus, altered osteoclast function modifies the regulation of B lymphopoiesis in the bone marrow (31). This is complementary to our studies showing that *Prrx1:Rarg*$^{\Delta/\Delta}$ male, but not female, mice had increased osteoclastogenesis and increased pro-B and pre-B lymphocyte numbers, suggesting that enhanced osteoclastogenesis may contribute to the B lymphocyte phenotype.

The increase in B lymphocyte precursors in male *Prrx1:Rarg*$^{\Delta/\Delta}$ mice (Fig. 6) contrasts to the reduced pre-B lymphocytes observed in male *Rarg*$^{-/-}$ and *nestin-Cre*$^{+}$*:Rarg*$^{\Delta/\Delta}$ mice, reduced pro-B cells in *Rarg*$^{-/-}$ mice and unchanged pro-B cells in *nestin-Cre*$^{+}$*:Rarg*$^{\Delta/\Delta}$ mice (9). Furthermore, *Osx1:Rarg*$^{\Delta/\Delta}$ mice had no alterations in the numbers of B lymphocytes in their

BM, spleen or PB (9). *Prrx1*- and *nestin*-expressing cells are distinct, non-overlapping populations in the BM, targeting limb bud and neural crest mesenchyme, respectively (9, 33, 59). As such, RARγ signaling appears to differentially regulate B lymphopoiesis in *Prrx1*- and *nestin*-*Cre*-targeted cells and these cells may form distinct B lymphocyte niches.

In this study, we identified that RARγ signaling in *Prrx1*-*Cre*-targeted mesenchymal cells is required for BM microenvironment development. Loss of *Rarg* in *Prrx1*-*Cre*-targeted cells impaired tibial longitudinal growth and caused a lower trabecular bone mass, however, the normal bone phenotype in *Osx1:Rarg*$^{\Delta/\Delta}$ mice suggested that this was not due to loss of *Rarg* in osteoblast progenitors or osteoblasts. *Prrx1:Rarg*$^{\Delta/\Delta}$ mice also exhibited a smaller growth plate, retained hypertrophic chondrocytes in epiphyseal trabecular bone and had defective endochondral bone formation with increased angiogenesis and altered trabecular osteoclastogenesis (in males) and osteoblastogenesis (in females). Furthermore, the increased osteoclastogenesis observed in *Prrx1:Rarg*$^{\Delta/\Delta}$ males was accompanied by increased numbers of pro-B and pre-B lymphocytes in the male mice, suggesting another link between osteoclasts and B lymphocytes. Collectively, our data identify that in limb bud-derived MSCs, RARγ is a key direct regulator of endochondral bone formation, and is an extrinsic regulator of angiogenesis, osteoclastogenesis and immature B lymphopoiesis in the bone marrow.

Author contributions

ACG and LEP designed the study. Experiments were performed and analyzed by ACG, VRS, BCI, LS, GT, MW, NAS, LEP. Data interpretation was performed by ACG, VRS, TJM, NAS and LEP. ACG and LEP drafted manuscript. ACG, VRS, TJM, NAS, and LEP revised manuscript. All authors approved the final manuscript.

Acknowledgments

The authors would like to thank the staff at the St Vincent's Bioresource Centre for caring for the animals used in this study, Ana Maluenda, Chacko Joseph, Diannita Kwang, Ingrid Poulton and Narelle McGregor for excellent technical assistance and Michael Thompson and Dijana Miljkovic in the SVI Flow Cytometry Facility for FACS-sorting cells for these studies. We thank Prof Pierre Chambon for providing us with the founders of the *Rarg* and *Rarg*$^{fl/fl}$ mice and Dr Andy McMahon for *Osx1-Cre* founder mice used in these studies. This research was supported in part by a project grant from the National Health and Medical Research Council (NHMRC, to LEP) and the Operational Infrastructure Support Program from the Victorian Government (to St. Vincent's Institute). LEP and NAS were supported by NHMRC Senior Research Fellowships.

References

1. Green AC, Poulton IJ, Vrahnas C, Hausler KD, Walkley CR, Wu JY, et al. RARgamma is a negative regulator of osteoclastogenesis. The Journal of steroid biochemistry and molecular biology. 2015;150:46-53.
2. Walkley CR, Olsen GH, Dworkin S, Fabb SA, Swann J, McArthur GA, et al. A microenvironment-induced myeloproliferative syndrome caused by retinoic acid receptor gamma deficiency. Cell. 2007;129(6):1097-110.
3. Green AC, Martin TJ, Purton LE. The role of vitamin A and retinoic acid receptor signaling in post-natal maintenance of bone. The Journal of steroid biochemistry and molecular biology. 2016;155(Pt A):135-46.
4. Lohnes D, Kastner P, Dierich A, Mark M, LeMeur M, Chambon P. Function of retinoic acid receptor gamma in the mouse. Cell. 1993;73(4):643-58.
5. Lufkin T, Lohnes D, Mark M, Dierich A, Gorry P, Gaub MP, et al. High postnatal lethality and testis degeneration in retinoic acid receptor alpha mutant mice. Proc Natl Acad Sci U S A. 1993;90(15):7225-9.
6. Purton LE, Dworkin S, Olsen GH, Walkley CR, Fabb SA, Collins SJ, et al. RARgamma is critical for maintaining a balance between hematopoietic stem cell self-renewal and differentiation. J Exp Med. 2006;203(5):1283-93.
7. Kastner P, Chan S. Function of RARalpha during the maturation of neutrophils. Oncogene. 2001;20(49):7178-85.
8. Dewamitta SR, Joseph C, Purton LE, Walkley CR. Erythroid-extrinsic regulation of normal erythropoiesis by retinoic acid receptors. British journal of haematology. 2014;164(2):280-5.
9. Joseph C, Nota C, Fletcher JL, Maluenda AC, Green AC, Purton LE. Retinoic Acid Receptor gamma Regulates B and T Lymphopoiesis via Nestin-Expressing Cells in the Bone Marrow and Thymic Microenvironments. Journal of immunology. 2016;196(5):2132-44.
10. Panaroni C, Fulzele K, Saini V, Chubb R, Pajevic PD, Wu JY. PTH Signaling in Osteoprogenitors Is Essential for B-Lymphocyte Differentiation and Mobilization. J Bone Miner Res. 2015;30(12):2273-86.
11. Wu JY, Purton LE, Rodda SJ, Chen M, Weinstein LS, McMahon AP, et al. Osteoblastic regulation of B lymphopoiesis is mediated by Gs{alpha}-dependent signaling pathways. Proc Natl Acad Sci U S A. 2008;105(44):16976-81.
12. Zhu J, Garrett R, Jung Y, Zhang Y, Kim N, Wang J, et al. Osteoblasts support B-lymphocyte commitment and differentiation from hematopoietic stem cells. Blood. 2007;109(9):3706-12.
13. Green AC, Kocovski P, Jovic T, Walia MK, Chandraratna RA, Martin TJ, et al. Retinoic acid receptor signalling directly regulates osteoblast and adipocyte differentiation from mesenchymal progenitor cells. Experimental cell research. 2017;350(1):284-97.
14. Rodda SJ, McMahon AP. Distinct roles for Hedgehog and canonical Wnt signaling in specification, differentiation and maintenance of osteoblast progenitors. Development. 2006;133(16):3231-44.
15. Logan M, Martin JF, Nagy A, Lobe C, Olson EN, Tabin CJ. Expression of Cre Recombinase in the developing mouse limb bud driven by a Prxl enhancer. Genesis. 2002;33(2):77-80.
16. Chapellier B, Mark M, Garnier JM, Dierich A, Chambon P, Ghyselinck NB. A conditional floxed (loxP-flanked) allele for the retinoic acid receptor gamma (RARgamma) gene. Genesis. 2002;32(2):95-8.

17. Bouxsein ML, Boyd SK, Christiansen BA, Guldberg RE, Jepsen KJ, Muller R. Guidelines for assessment of bone microstructure in rodents using micro-computed tomography. J Bone Miner Res. 2010;25(7):1468-86.
18. Sims NA, Brennan K, Spaliviero J, Handelsman DJ, Seibel MJ. Perinatal testosterone surge is required for normal adult bone size but not for normal bone remodeling. American journal of physiology Endocrinology and metabolism. 2006;290(3):E456-62.
19. Dempster DW, Compston JE, Drezner MK, Glorieux FH, Kanis JA, Malluche H, et al. Standardized nomenclature, symbols, and units for bone histomorphometry: a 2012 update of the report of the ASBMR Histomorphometry Nomenclature Committee. J Bone Miner Res. 2013;28(1):2-17.
20. Singbrant S, Russell MR, Jovic T, Liddicoat B, Izon DJ, Purton LE, et al. Erythropoietin couples erythropoiesis, B-lymphopoiesis, and bone homeostasis within the bone marrow microenvironment. Blood. 2011;117(21):5631-42.
21. Arthur A, Panagopoulos RA, Cooper L, Menicanin D, Parkinson IH, Codrington JD, et al. EphB4 enhances the process of endochondral ossification and inhibits remodeling during bone fracture repair. J Bone Miner Res. 2013;28(4):926-35.
22. Sims NA, Clement-Lacroix P, Da Ponte F, Bouali Y, Binart N, Moriggl R, et al. Bone homeostasis in growth hormone receptor-null mice is restored by IGF-I but independent of Stat5. The Journal of clinical investigation. 2000;106(9):1095-103.
23. Poulton Ingrid J, McGregor Narelle E, Pompolo S, Walker Emma C, Sims Natalie A. Contrasting roles of leukemia inhibitory factor in murine bone development and remodeling involve region‐specific changes in vascularization. Journal of Bone and Mineral Research. 2011;27(3):586-95.
24. Parra ER, Uraoka N, Jiang M, Cook P, Gibbons D, Forget M-A, et al. Validation of multiplex immunofluorescence panels using multispectral microscopy for immune-profiling of formalin-fixed and paraffin-embedded human tumor tissues. Scientific Reports. 2017;7(1):13380.
25. Nolan E, Savas P, Policheni AN, Darcy PK, Vaillant F, Mintoff CP, et al. Combined immune checkpoint blockade as a therapeutic strategy for BRCA1-mutated breast cancer. Sci Transl Med. 2017;9(393).
26. Askmyr M, White KE, Jovic T, King HA, Quach JM, Maluenda AC, et al. Ciliary neurotrophic factor has intrinsic and extrinsic roles in regulating B cell differentiation and bone structure. Sci Rep. 2015;5:15529.
27. Quach JM, Askmyr M, Jovic T, Baker EK, Walsh NC, Harrison SJ, et al. Myelosuppressive therapies significantly increase pro-inflammatory cytokines and directly cause bone loss. J Bone Miner Res. 2015;30(5):886-97.
28. Martin TJ. Historically significant events in the discovery of RANK/RANKL/OPG. World J Orthop. 2013;4(4):186-97.
29. Williams JA, Kondo N, Okabe T, Takeshita N, Pilchak DM, Koyama E, et al. Retinoic acid receptors are required for skeletal growth, matrix homeostasis and growth plate function in postnatal mouse. Dev Biol. 2009;328(2):315-27.
30. Nagasawa T. Microenvironmental niches in the bone marrow required for B-cell development. Nature reviews Immunology. 2006;6(2):107-16.
31. Green AC, Rudolph-Stringer V, Chantry AD, Wu JY, Purton LE. Mesenchymal lineage cells and their importance in B lymphocyte niches. Bone. 2017.
32. Poulton IJ, McGregor NE, Pompolo S, Walker EC, Sims NA. Contrasting roles of leukemia inhibitory factor in murine bone development and remodeling involve region-specific changes in vascularization. J Bone Miner Res. 2012;27(3):586-95.

33. Greenbaum A, Hsu YM, Day RB, Schuettpelz LG, Christopher MJ, Borgerding JN, et al. CXCL12 in early mesenchymal progenitors is required for haematopoietic stem-cell maintenance. Nature. 2013;495(7440):227-30.
34. Zhong ZA, Kot A, Lay YE, Zhang H, Jia J, Lane NE, et al. Sex-Dependent, Osteoblast Stage-Specific Effects of Progesterone Receptor on Bone Acquisition. J Bone Miner Res. 2017.
35. Maes C, Kobayashi T, Selig MK, Torrekens S, Roth SI, Mackem S, et al. Osteoblast precursors, but not mature osteoblasts, move into developing and fractured bones along with invading blood vessels. Dev Cell. 2010;19(2):329-44.
36. Rankin EB, Wu C, Khatri R, Wilson TL, Andersen R, Araldi E, et al. The HIF signaling pathway in osteoblasts directly modulates erythropoiesis through the production of EPO. Cell. 2012;149(1):63-74.
37. Chen J, Shi Y, Regan J, Karuppaiah K, Ornitz DM, Long F. Osx-Cre targets multiple cell types besides osteoblast lineage in postnatal mice. PLoS One. 2014;9(1):e85161.
38. Fosang AJ, Golub SB, East CJ, Rogerson FM. Abundant LacZ activity in the absence of Cre expression in the normal and inflamed synovium of adult Col2a1-Cre; ROSA26RLacZ reporter mice. Osteoarthritis Cartilage. 2013;21(2):401-4.
39. Sakai K, Hiripi L, Glumoff V, Brandau O, Eerola R, Vuorio E, et al. Stage-and tissue-specific expression of a Col2a1-Cre fusion gene in transgenic mice. Matrix Biol. 2001;19(8):761-7.
40. Tonna S, Poulton IJ, Taykar F, Ho PW, Tonkin B, Crimeen-Irwin B, et al. Chondrocytic ephrin B2 promotes cartilage destruction by osteoclasts in endochondral ossification. Development. 2016;144(3):530.
41. Rauch F, Travers R, Plotkin H, Glorieux FH. The effects of intravenous pamidronate on the bone tissue of children and adolescents with osteogenesis imperfecta. Journal of Clinical Investigation. 2002;110(9):1293-9.
42. Kang JH, Choi NK, Kang SJ, Yang SY, Ko HM, Jung JY, et al. Alendronate affects cartilage resorption by regulating vascular endothelial growth factor expression in rats. Anat Rec (Hoboken). 2010;293(5):786-93.
43. Dirckx N, Van Hul M, Maes C. Osteoblast recruitment to sites of bone formation in skeletal development, homeostasis, and regeneration. Birth Defects Res C Embryo Today. 2013;99(3):170-91.
44. Gerber HP, Vu TH, Ryan AM, Kowalski J, Werb Z, Ferrara N. VEGF couples hypertrophic cartilage remodeling, ossification and angiogenesis during endochondral bone formation. Nat Med. 1999;5(6):623-8.
45. Krauth MT, Simonitsch I, Aichberger KJ, Mayerhofer M, Sperr WR, Sillaber C, et al. Immunohistochemical detection of VEGF in the bone marrow of patients with chronic myeloid leukemia and correlation with the phase of disease. Am J Clin Pathol. 2004;121(4):473-81.
46. Engsig MT, Chen QJ, Vu TH, Pedersen AC, Therkidsen B, Lund LR, et al. Matrix metalloproteinase 9 and vascular endothelial growth factor are essential for osteoclast recruitment into developing long bones. J Cell Biol. 2000;151(4):879-89.
47. Maes C, Carmeliet P, Moermans K, Stockmans I, Smets N, Collen D, et al. Impaired angiogenesis and endochondral bone formation in mice lacking the vascular endothelial growth factor isoforms VEGF164 and VEGF188. Mechanisms of development. 2002;111(1-2):61-73.
48. Bonsi L, Pierdomenico L, Biscardi M, Marchionni C, Gavazzi S, Fossati V, et al. Constitutive and stimulated production of VEGF by human megakaryoblastic cell lines: effect on proliferation and signaling pathway. Int J Immunopathol Pharmacol. 2005;18(3):445-55.
49. Mohle R, Green D, Moore MA, Nachman RL, Rafii S. Constitutive production and thrombin-induced release of vascular endothelial growth factor by human megakaryocytes and platelets. Proc Natl Acad Sci U S A. 1997;94(2):663-8.

50. Yao S, Liu D, Pan F, Wise GE. Effect of vascular endothelial growth factor on RANK gene expression in osteoclast precursors and on osteoclastogenesis. Arch Oral Biol. 2006;51(7):596-602.
51. Yang Q, McHugh KP, Patntirapong S, Gu X, Wunderlich L, Hauschka PV. VEGF enhancement of osteoclast survival and bone resorption involves VEGF receptor-2 signaling and beta3-integrin. Matrix Biol. 2008;27(7):589-99.
52. Cordeiro Gomes A, Hara T, Lim VY, Herndler-Brandstetter D, Nevius E, Sugiyama T, et al. Hematopoietic Stem Cell Niches Produce Lineage-Instructive Signals to Control Multipotent Progenitor Differentiation. Immunity. 2016;45(6):1219-31.
53. Ding L, Morrison SJ. Haematopoietic stem cells and early lymphoid progenitors occupy distinct bone marrow niches. Nature. 2013;495(7440):231-5.
54. Mackarehtschian K, Hardin JD, Moore KA, Boast S, Goff SP, Lemischka IR. Targeted disruption of the flk2/flt3 gene leads to deficiencies in primitive hematopoietic progenitors. Immunity. 1995;3(1):147-61.
55. Sitnicka E, Brakebusch C, Martensson IL, Svensson M, Agace WW, Sigvardsson M, et al. Complementary signaling through flt3 and interleukin-7 receptor alpha is indispensable for fetal and adult B cell genesis. J Exp Med. 2003;198(10):1495-506.
56. Murata K, Kitaori T, Oishi S, Watanabe N, Yoshitomi H, Tanida S, et al. Stromal cell-derived factor 1 regulates the actin organization of chondrocytes and chondrocyte hypertrophy. PLoS One. 2012;7(5):e37163.
57. Blin-Wakkach C, Wakkach A, Sexton PM, Rochet N, Carle GF. Hematological defects in the oc/oc mouse, a model of infantile malignant osteopetrosis. Leukemia. 2004;18(9):1505-11.
58. Mansour A, Anginot A, Mancini SJ, Schiff C, Carle GF, Wakkach A, et al. Osteoclast activity modulates B-cell development in the bone marrow. Cell Res. 2011;21(7):1102-15.
59. Isern J, Garcia-Garcia A, Martin AM, Arranz L, Martin-Perez D, Torroja C, et al. The neural crest is a source of mesenchymal stem cells with specialized hematopoietic stem cell niche function. Elife. 2014;3:e03696.

Figure 1: *Rarg*$^{-/-}$ mice have less trabecular bone and shorter tibiae than *Rarg*$^{+/+}$ mice

Tibial trabecular bone structure and length was analyzed by μCT in 12-week-old male and female *Rarg*$^{+/+}$ vs. *Rarg*$^{-/-}$ mice. The graphs show trabecular bone volume (BV/TV; A), trabecular thickness (Tb.Th; B), trabecular separation (Tb.Sp; C) and trabecular number (Tb.N; D). Representative reconstructed tibiae images for male (E-F) and female (G-H) mice. Graph (I) shows tibial lengths for 12-week-old mice. Male (n=10), female *Rarg*$^{+/+}$ (n=8) and *Rarg*$^{-/-}$ (n=6) mice. **p<0.01, ***p<0.001 and ****p<0.0001 (unpaired two-tailed Student's t-test).

Figure 2: *Rarg*$^{-/-}$ mice have thinner cortical bone and narrower tibiae than *Rarg*$^{+/+}$ mice

Tibial cortical bone structure was analyzed by μCT in 12-week-old male and female *Rarg*$^{+/+}$ vs. *Rarg*$^{-/-}$ mice. The graphs show cortical bone thickness (Ct.Th; A), marrow area (Ma.Ar; B), cortical area (Ct.Ar; C) and periosteal perimeter (Ps.Pm; D). Males (n=10), female *Rarg*$^{+/+}$ (n=8) and *Rarg*$^{-/-}$ (n=6) mice. **p<0.01, ***p<0.001 and ****p<0.0001 (unpaired two-tailed Student's t-test).

Figure 3: 12-week-old *Osx1:Rarg*$^{\Delta/\Delta}$ mice do not exhibit a defect in trabecular bone

Tibial trabecular bone structure was analyzed by μCT in 12-week-old male *Osx1:Rarg*$^{+/+}$ (n=7) vs. *Osx1:Rarg*$^{\Delta/\Delta}$ (n=12) mice. The graphs show trabecular bone volume (BV/TV; A), trabecular thickness (Tb.Th; B), trabecular separation (Tb.Sp; C) and trabecular number (Tb.N; D). Representative reconstructed images of trabecular bone are shown for *Osx1:Rarg*$^{+/+}$ (E) and *Osx1:Rarg*$^{\Delta/\Delta}$ (F). *p<0.05, **p<0.01, and ***p<0.001 (unpaired two-tailed Student's t-test).

Figure 4: *Prrx1:Rarg*$^{\Delta/\Delta}$ mice have less trabecular bone than *Prrx1:Rarg*$^{+/+}$ mice

Tibial trabecular bone structure was analyzed by μCT in 12-week-old male and female *Prrx1:Rarg*$^{+/+}$ vs. *Prrx1:Rarg*$^{\Delta/\Delta}$ mice. The graphs show trabecular bone volume (BV/TV; A), trabecular thickness (Tb.Th; B), trabecular separation (Tb.Sp; C), trabecular number (Tb.N; D)

and tibial length (I). Representative reconstructed images of trabecular bone are shown for males (E-F) and females (G-H). Male *Prrx1:Rarg*$^{+/+}$ (n=11), *Prrx1:Rarg*$^{\Delta/\Delta}$ (n=12), female *Prrx1:Rarg*$^{+/+}$ (n=13) and *Prrx1:Rarg*$^{\Delta/\Delta}$ (n=15) mice. *p<0.05, **p<0.01, and ***p<0.001 (unpaired two-tailed Student's t-test).

Figure 5: *Prrx1:Rarg*$^{\Delta/\Delta}$ male mice have greater osteoclastogenesis and females have more osteoid surface and osteoblasts compared to *Prrx1:Rarg*$^{+/+}$ mice

Histomorphometry of the tibial secondary spongiosa was performed on non-decalcified plastic embedded bones (A-G), and decalcified paraffin embedded bones (H-L). The graphs show the osteoid volume/bone volume (OV/BV; A), osteoid surface/bone surface (OS/BS; B), osteoid thickness (O.Th; C), osteoblast surface/bone surface (Ob.S/BS; D), number of osteoblasts/bone perimeter (N.Ob/B.Pm; E), osteoclast surface/ bone surface (Oc.S/BS; F) and number of osteoclasts/bone perimeter (N.Oc/B.Pm; G). Male *Prrx1:Rarg*$^{+/+}$ (n=9), *Prrx1:Rarg*$^{\Delta/\Delta}$ (n=10), female *Prrx1:Rarg*$^{+/+}$ (n=8) and *Prrx1:Rarg*$^{\Delta/\Delta}$ (n=10) mice. Graph (H) shows the number of hypertrophic chondrocyte islands in epiphyseal bone, representative images (I-K) of male *Prrx1:Rarg*$^{+/+}$ (I) and *Prrx1:Rarg*$^{\Delta/\Delta}$ (J-K) tibiae showing chondrocyte islands (black arrowheads) and graph (L) shows growth plate width in tibiae; scale bars are 500 μm (I-J) and 100 μm (K). **Graph (M) shows the width of the proliferative zone and graph (N) shows the width of the hypertrophic zone in 20-day old tibiae, representative images (O, P) of male *Prrx1:Rarg*$^{+/+}$ (O) and *Prrx1:Rarg*$^{\Delta/\Delta}$ (P) tibiae. HZ= hypertrophic zone, PZ= proliferative zone, GZ= germinal zone.** Male *Prrx1:Rarg*$^{+/+}$ (n=7), *Prrx1:Rarg*$^{\Delta/\Delta}$ (n=6), female *Prrx1:Rarg*$^{+/+}$ (n=6) and *Prrx1:Rarg*$^{\Delta/\Delta}$ (n=9) mice. *p<0.05, **p<0.01 and ***p<0.001 (unpaired two-tailed Student's t-test).

Figure 6: *Prrx1:Rarg*$^{\Delta/\Delta}$ male mice have increased pro-B and pre-B lymphocytes in the bone marrow compared to *Prrx1:Rarg*$^{+/+}$ male mice

Graph (A) shows the number of bone marrow (BM) leukocytes per femur in *Prrx1:Rarg*$^{+/+}$ and *Prrx1:Rarg*$^{\Delta/\Delta}$ mice. Representative flow cytometry plots of B lymphocytes subsets (B-C). The graphs show the numbers of cells per femur for: $B220^{+}IgM^{-}$ and $B220^{+}IgM^{+}$ B lymphocytes (D), $CD19^{-}CD43^{-}$ pre-pro-B lymphocytes, $CD19^{+}CD43^{+}$ pro-B lymphocytes and $CD19^{+}CD43^{-}$ pre-B lymphocytes (E). Male *Prrx1:Rarg*$^{+/+}$ (n=10), *Prrx1:Rarg*$^{\Delta/\Delta}$ (n=12), female *Prrx1:Rarg*$^{+/+}$ (n=13) and *Prrx1:Rarg*$^{\Delta/\Delta}$ (n=12) mice. Schematic (I) shows stages of B lymphopoiesis highlighting pro-B and pre-B stages altered in *Prrx1:Rarg*$^{\Delta/\Delta}$ males; hematopoietic stem cell (HSC), common lymphoid progenitor (CLP). qPCR of *Cxcl12* (G), *Flt3l* (H), *Tnfrsf11b* (I) and *Vegfa* (J) gene expression in whole BM cells from *Prrx1:Rarg*$^{+/+}$ and *Prrx1:Rarg*$^{\Delta/\Delta}$ male mice (n=4 mice/group). The expression of these transcripts, including secreted (sec) and membrane-bound (mem) forms of *Kitl* are also shown in FACS-sorted MSCs (K) and osteoblast lineage cells (L) obtained from *Prrx1:Rarg*$^{\Delta/\Delta}$ male mice, with expression normalized to cells sorted from *Prrx1:Rarg*$^{+/+}$ male mice (n=3-5 separate experiments/group). *p<0.05, **p<0.01, and ***p<0.001 (unpaired two-tailed Student's t-test).

Figure 7: *Prrx1:Rarg*$^{\Delta/\Delta}$ mice have smaller BM sinusoidal vessels and females have more sinusoids and increased Vegf-a expression in megakaryocytes

Immunohistochemistry of VEGFR-3+ sinusoidal vessels in the secondary spongiosa of *Prrx1:Rarg*$^{+/+}$ and *Prrx1:Rarg*$^{\Delta/\Delta}$ mice. The graphs show the number of sinusoids/ marrow area (N.sinusoids/Ma.Ar; A), sinusoid area/ sinusoid (Sinusoid.Ar/sinusoid; B), sinusoid area/ marrow area (sinusoid Ar/Ma.Ar; C), and sinusoid perimeter/ marrow area (sinusoid Pm./Ma.Ar; D). Representative images (E-H) of VEGFR-3-stained BM sections, showing sinusoids (s), bone marrow (bm) and trabecular bone (tb), scale bars are 100 μm.

Representative images showing EYFP and Vegf-a stained BM sections obtained from (I) Prrx1:Rarg$^{+/+}$ and (J) Prrx1:Rarg$^{\Delta/\Delta}$ mice. The images show growth plate and bone marrow regions separately, with enlargements of each region in the insets. Scale bars are 100 µm. (K) Flow cytometry quantitation of the proportion of CD41+ megakaryocytes in the BM of *Prrx1:Rarg*$^{+/+}$ and *Prrx1:Rarg*$^{\Delta/\Delta}$ mice. Male *Prrx1:Rarg*$^{+/+}$ (n=8), *Prrx1:Rarg*$^{\Delta/\Delta}$ (n=8), female *Prrx1:Rarg*$^{+/+}$ (n=8) and *Prrx1:Rarg*$^{\Delta/\Delta}$ (n=9) mice. *p<0.05 and *p<0.05 (unpaired two-tailed Student's t-test).

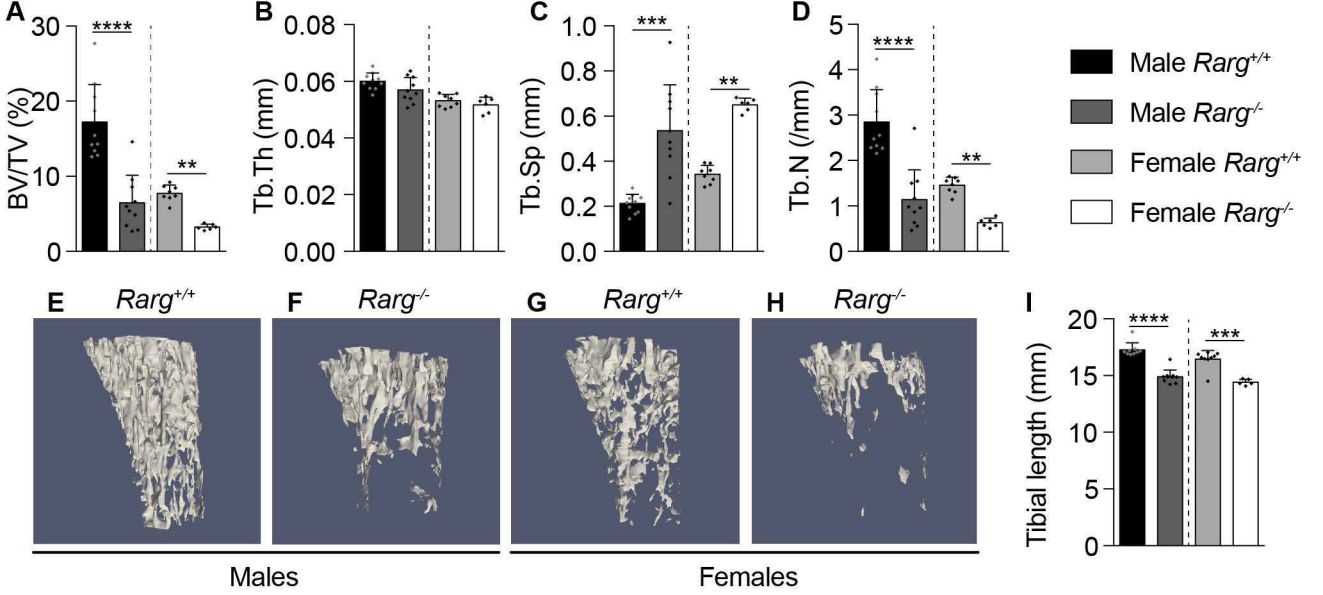
A
BV/TV (%)
30
20
10
0
****
**
B
Tb.Th (mm)
0.08
0.06
0.04
0.02
0.00
C
Tb.Sp (mm)
1.0
0.8
0.6
0.4
0.2
0.0
***
**
D
Tb.N (/mm)
5
4
3
2
1
0
****
**
Male Rarg+/+
Male Rarg-/-
Female Rarg+/+
Female Rarg-/-
E Rarg+/+
F Rarg-/-
G Rarg+/+
H Rarg-/-
Males
Females
I
Tibial length (mm)
20
15
10
5
0
****
***

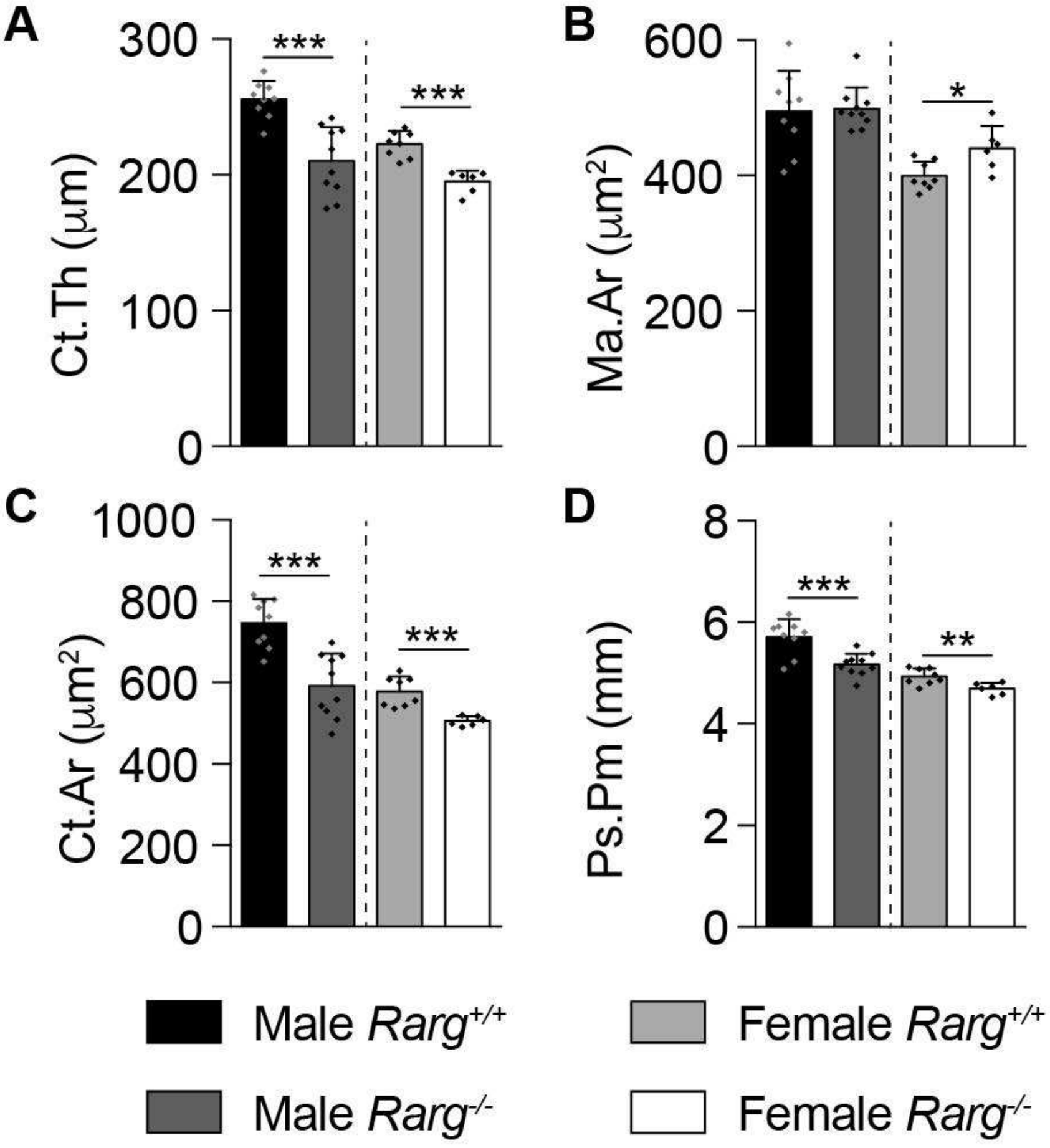
A
Ct.Th (μm)
300
200
100
0
***
***
B
Ma.Ar (μm²)
600
400
200
0
*
C
Ct.Ar (μm²)
1000
800
600
400
200
0
***
***
D
Ps.Pm (mm)
8
6
4
2
0
***
**
Male Rarg+/+
Male Rarg-/-
Female Rarg+/+
Female Rarg-/-

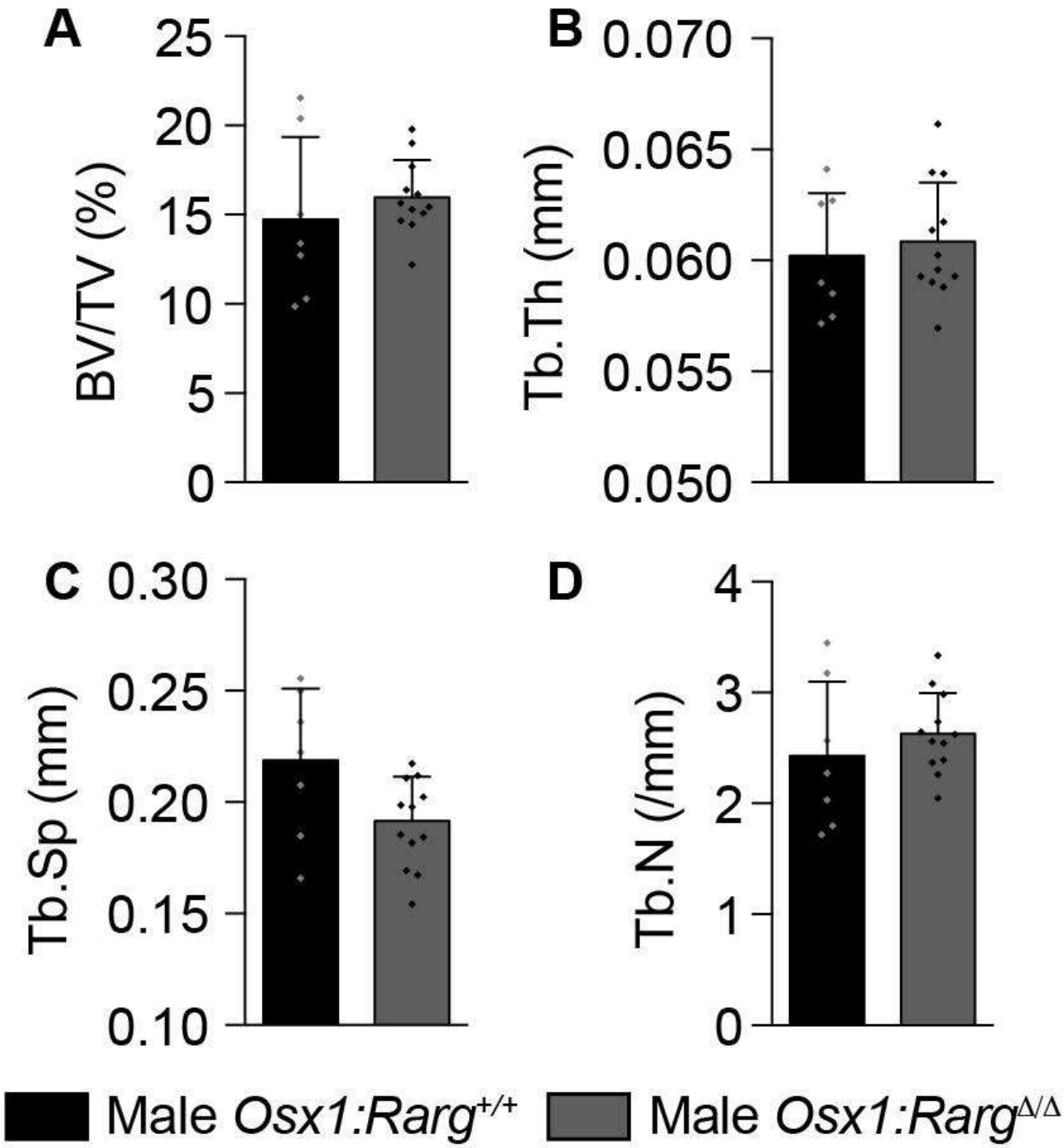
A
BV/TV (%)
25
20
15
10
5
0
B
Tb.Th (mm)
0.070
0.065
0.060
0.055
0.050
C
Tb.Sp (mm)
0.30
0.25
0.20
0.15
0.10
D
Tb.N (/mm)
4
3
2
1
0
Male Osx1:Rarg+/+
Male Osx1:RargΔ/Δ

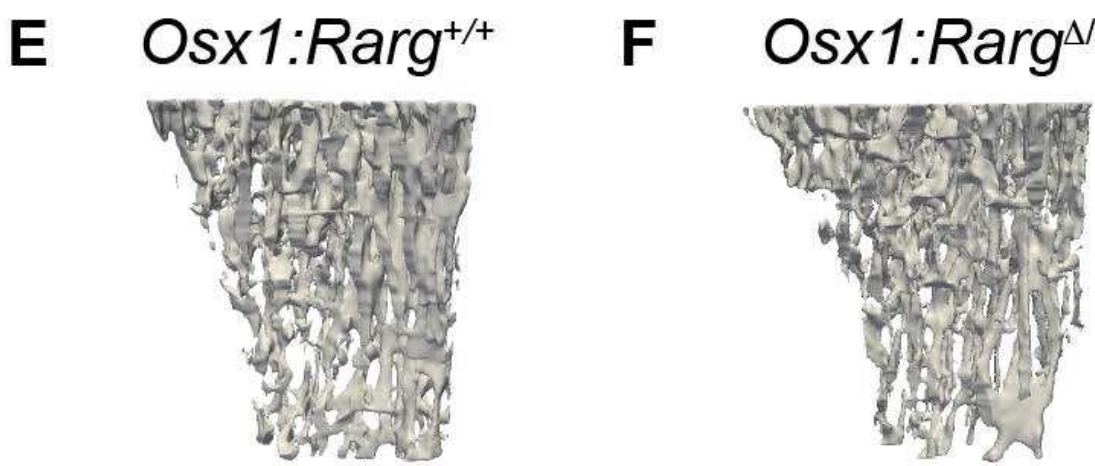
E
Osx1:Rarg+/+
F
Osx1:RargΔ/Δ

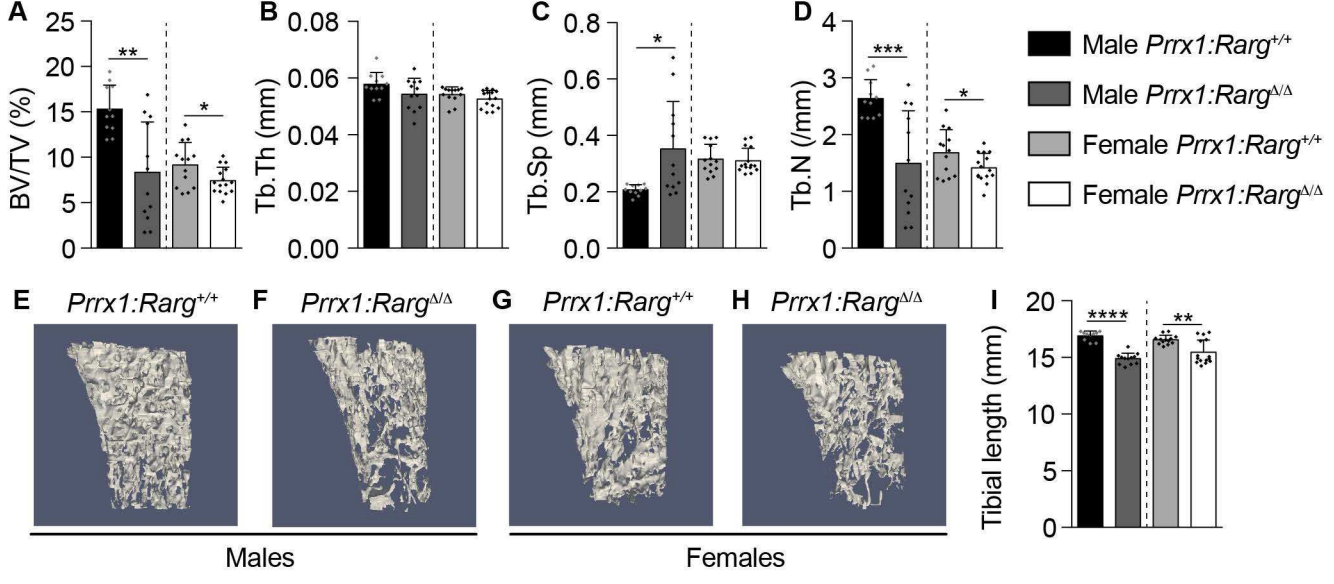
A
BV/TV (%)
25
20
15
10
5
0
**
*
B
Tb.Th (mm)
0.08
0.06
0.04
0.02
0.00
C
Tb.Sp (mm)
0.8
0.6
0.4
0.2
0.0
*
D
Tb.N (/mm)
4
3
2
1
0
***
*
Male Prrx1:Rarg+/+
Male Prrx1:RargΔ/Δ
Female Prrx1:Rarg+/+
Female Prrx1:RargΔ/Δ
E
Prrx1:Rarg+/+
F
Prrx1:RargΔ/Δ
G
Prrx1:Rarg+/+
H
Prrx1:RargΔ/Δ
Males
Females
I
Tibial length (mm)
20
15
10
5
0
****
**

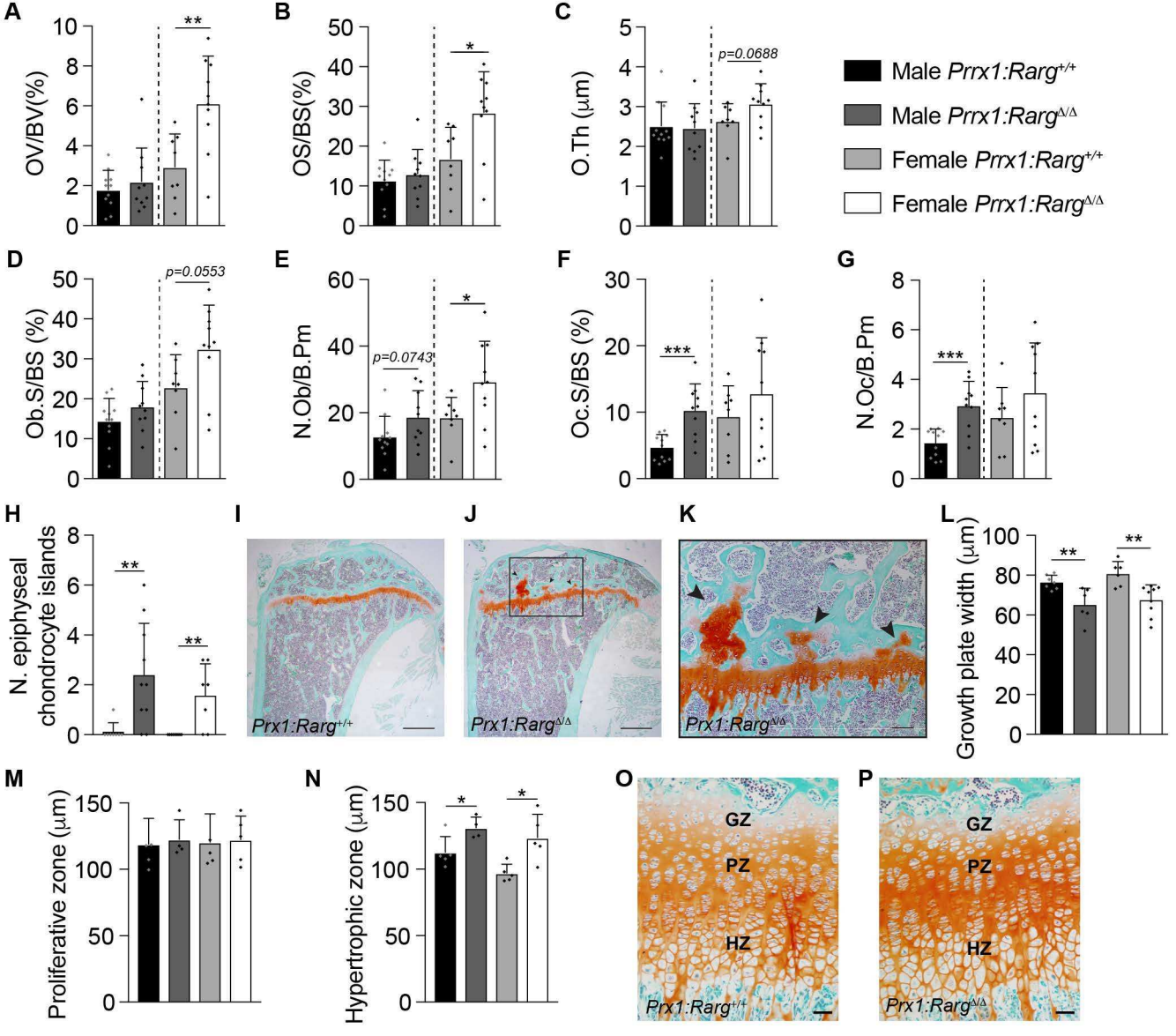
A
OV/BV(%)
B
OS/BS(%)
C
O.Th (μm)
p=0.0688
Male Prrx1:Rarg+/+
Male Prrx1:RargΔ/Δ
Female Prrx1:Rarg+/+
Female Prrx1:RargΔ/Δ
D
Ob.S/BS (%)
p=0.0553
E
N.Ob/B.Pm
p=0.0743
F
Oc.S/BS (%)
G
N.Oc/B.Pm
H
N. epiphyseal chondrocyte islands
I
Prx1:Rarg+/+
J
Prx1:RargΔ/Δ
K
Prx1:RargΔ/Δ
L
Growth plate width (μm)
M
Proliferative zone (μm)
N
Hypertrophic zone (μm)
O
GZ
PZ
HZ
Prx1:Rarg+/+
P
GZ
PZ
HZ
Prx1:RargΔ/Δ

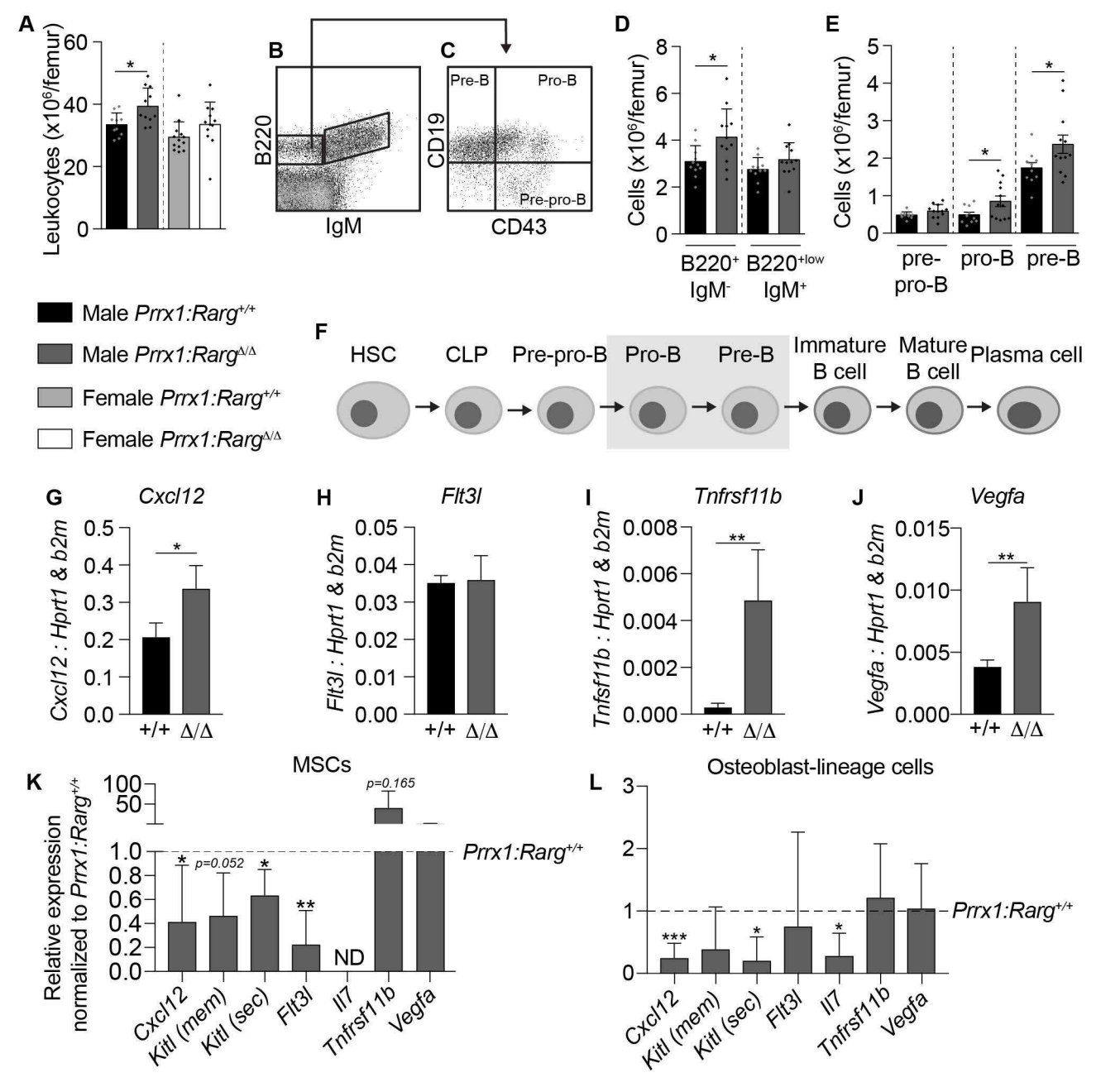
A
Leukocytes (x10⁶/femur)
B
B220
IgM
C
CD19
CD43
Pre-B
Pro-B
Pre-pro-B
D
Cells (x10⁶/femur)
B220⁺ IgM⁻
B220^+low IgM⁺
E
Cells (x10⁶/femur)
pre-pro-B
pro-B
pre-B
Male Prrx1:Rarg+/+
Male Prrx1:RargΔ/Δ
Female Prrx1:Rarg+/+
Female Prrx1:RargΔ/Δ
F
HSC
CLP
Pre-pro-B
Pro-B
Pre-B
Immature B cell
Mature B cell
Plasma cell
G
Cxcl12
Cxcl12 : Hprt1 & b2m
H
Flt3l
Flt3l : Hprt1 & b2m
I
Tnfrsf11b
Tnfrsf11b : Hprt1 & b2m
J
Vegfa
Vegfa : Hprt1 & b2m
+/+
Δ/Δ
K
MSCs
Relative expression normalized to Prrx1:Rarg+/+
p=0.165
p=0.052
Prrx1:Rarg+/+
ND
Cxcl12
Kitl (mem)
Kitl (sec)
Flt3l
Il7
Tnfrsf11b
Vegfa
L
Osteoblast-lineage cells
Prrx1:Rarg+/+
Cxcl12
Kitl (mem)
Kitl (sec)
Flt3l
Il7
Tnfrsf11b
Vegfa

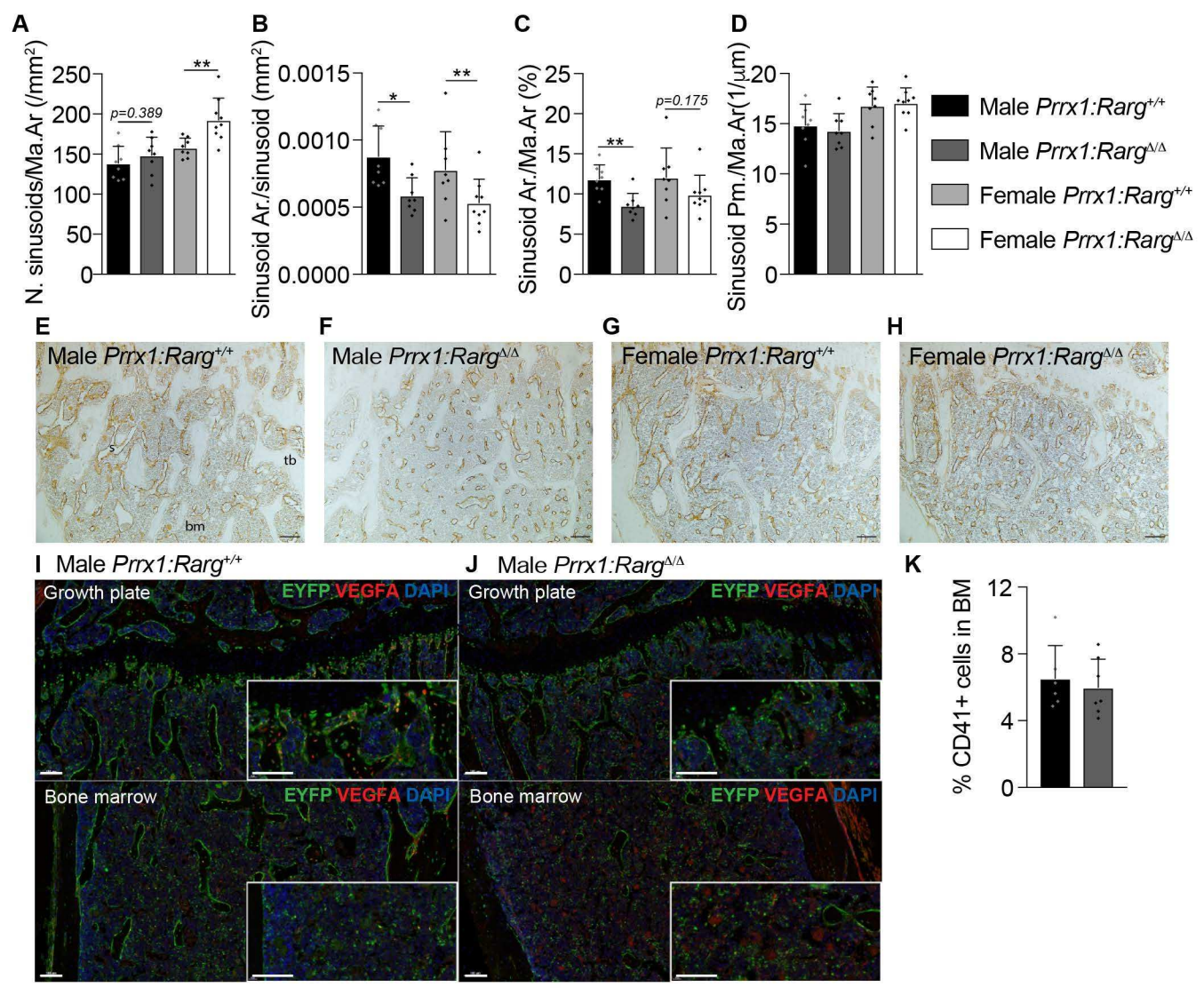
A
N. sinusoids/Ma.Ar (/mm²)
250
200
150
100
50
0
p=0.389
**
B
Sinusoid Ar./sinusoid (mm²)
0.0015
0.0010
0.0005
0.0000
*
**
C
Sinusoid Ar./Ma.Ar (%)
25
20
15
10
5
0
**
p=0.175
D
Sinusoid Pm./Ma.Ar(1/µm)
20
15
10
5
0
Male Prrx1:Rarg+/+
Male Prrx1:RargΔ/Δ
Female Prrx1:Rarg+/+
Female Prrx1:RargΔ/Δ
E
Male Prrx1:Rarg+/+
s
tb
bm
F
Male Prrx1:RargΔ/Δ
G
Female Prrx1:Rarg+/+
H
Female Prrx1:RargΔ/Δ
I Male Prrx1:Rarg+/+
Growth plate
EYFP VEGFA DAPI
Bone marrow
EYFP VEGFA DAPI
J Male Prrx1:RargΔ/Δ
Growth plate
EYFP VEGFA DAPI
Bone marrow
EYFP VEGFA DAPI
K
% CD41+ cells in BM
12
8
4
0